Helicopter Ground Resonance Phenomenon With Blade Stiffness Dissimilarities: Experimental and Theoretical Developments

Leonardo Sanches, Guilhem Michon, Alain Berlioz, Daniel Alazard

Helicopter Ground Resonance Phenomenon With Blade Stiffness Dissimilarities: Experimental and Theoretical Developments

Leonardo Sanches[1]
Faculty of Mechanical Engineering, Federal University of Uberlandia, Santa Monica, Uberlandia, MG 38400-902, Brazil
Guilhem Michon
Institut Clémant Ader, ISAE, Université de Toulouse, Toulouse 31055, France
Alain Berlioz
Insitut Clémant Ader, UPS, Université de Toulouse, Toulouse 31077, France
Daniel Alazard
Département Mathématique,
Informatique et Automatique, ISAE, Université de Toulouse, Toulouse 31055, France

Recent works have studied ground resonance in helicopters under the aging or damage effects. Indeed, blade lead-lag stiffness may vary randomly with time and differ from blade to blade. The influence of stiffness dissimilarities between blades on the stability of the ground resonance phenomenon was determined through numerical investigations into the periodic equations of motion, treated using Floquet's theory. A stability chart high-lights the appearance of new instability zones as a function of the perturbation intro-duced on the lead-lag stiffness of one blade. In order to validate the theoretical results, a new experimental setup was designed and developed. The ground resonance instabilities were investigated using different rotors and the boundaries of stability were determined. A good correlation between both theoretical and experimental results was obtained and the new instability zones, found in asymmetric rotors, were verified experimentally. The temporal responses of the measured signals highlighted the exponential divergence in the instability zones.

1 Introduction

The ground resonance phenomenon consists in potential instability, at certain critical rotor speeds, as a result of the coalescence between the fuselage and cyclic rotor modes of vibrations over the landing skids of a helicopter while it is on the ground [1,2].

Studies carried out on this subject have concluded that the use of linearized periodic equations of motions provide accurate frequency prediction of critical zones for articulated, bearingless or hingeless rotors [3–5]. In all these investigations, only isotropic rotor configurations (all blades having the same mechanical properties) have been considered.

Nevertheless, this assumption is no longer valid when considering the helicopter under the aging or damage effects. Indeed, due to these effects, the stiffness properties of blades may vary randomly with time, and differ from blade to blade (i.e., anisotropic rotor). The study of ground resonance in helicopters with anisotropic rotors is very interesting from a practical point of view, as it enables helicopter maintenance interventions to be optimized by avoiding the instabilities which characterize the phenomenon.

Wang and Chopra [2] examined the influence of the aging effects on the ground resonance phenomenon, by assuming a slight lead-lag stiffness asymmetry of $\pm 5\%$ on one blade. The analysis, conducted using Floquet's theory, verifies an enlargement of unstable zones. Their mechanical model does not considers aerodynamics efforts.

The study of balanced dissimilarities (maximum attained level of asymmetry is 40%) in rotors containing aerodynamic efforts has done by Gandhi and Malovrh [6]. Several of his other publications has focused on the stability augmentation of the aeromechanical phenomena through passive and active control techniques [7,8].

Sanches et al. [9] in his recent work has gone further on the analysis of the ground resonance phenomenon in helicopters with anisotropic rotors done by Wang [2]. A parametric study is developed considering high level of stiffness asymmetries on different blades. Stability charts, obtained with the Floquet's theory, show the complex evolution of the instability zones with respect to the asymmetries introduced, evidencing the appearance of new critical zones.

Further analysis on the ground resonance phenomenon with dissimilar blades was carried out using perturbation technique [10]. The weakly coupled rotor-fuselage dynamic system, by the periodic terms, is treated as a parametrically excited system. The stability analysis highlighted the existence of first and second order parametric instabilities, proposing an explanation for the appearance of new critical regions when high blade stiffness asymmetry (i.e., bigger than 20%) is reached.

It should be noted that, in order to verify all the possible instability zones, the dissipative efforts provided by viscous dampers were not considered in the mechanical model.

The present paper aims to validate experimentally the theoretical results, verifying the appearance of new instability regions in helicopters under the aging or damage effects (i.e., anisotropic rotor). For this purpose, a new experimental setup designed and described. Isotropic and anisotropic rotor configurations are analyzed. The boundaries of instability, determined by means of experimental tests, are compared with those predicted when using Floquet's theory.

2 Ground Resonance: Derivation of Equations and Stability Analysis

2.1 Derivation of Equations. Figure 1 shows the mechanical model considered for the study of the ground resonance phenomenon in helicopters with a four-bladed rotor and under the aging effects. It is based on the one used by Sanches [9,10], nevertheless taking into account the presence of viscous dampers on the fuselage oscillations and the blade lead-lag rotations.

[1]Corresponding author.

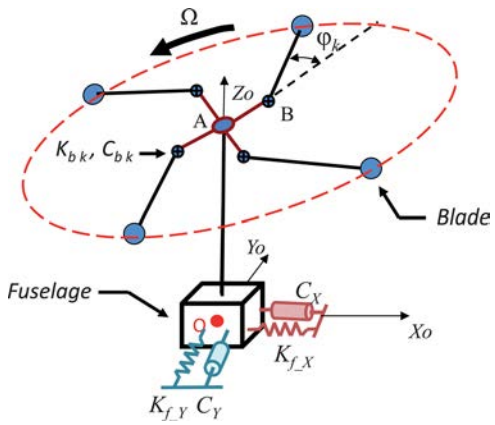

Fig. 1 Representation of the mechanical model

The fuselage movements are described as a function of its longitudinal and lateral displacements, $x(t)$ and $y(t)$, respectively. The fuselage, with mass m_f, is considered as a rigid body. The stiffness of springs, situated along x and y directions, respectively, is given by K_{fX} and K_{fY}. They represent the stiffness provided by the landing skids, while the helicopter is on the ground.

Similarly, the damping effects, modeled as a viscous damper, have coefficients equal to C_X and C_Y in the longitudinal and lateral directions of the fuselage, respectively. The center of mass of the fuselage (point O) of the helicopter at equilibrium position is coincident with the origin of the inertial reference frame (X_0, Y_0, Z_0).

The rotor head system is composed of one rigid rotor hub and an assembly of N_b rigid blades. Each kth blade has mass m_{bk} and a moment of inertia I_{zbk} around the z-axis located at its center of mass. The radius of gyration is defined by length b. Each kth blade has an in-plane lead-lag motion defined by $\varphi_k(t)$ and an azimuth angle defined as $\zeta_k = 2\pi(k-1)/N_b$ with respect to the x-axis. A torsional spring and viscous damper are considered on each blade hinge (point B) with a spring stiffness and viscous damping coefficient of K_{bk} and C_{bk}, respectively.

The origin of a rotational reference frame (x, y, z) is parallel to the inertial one and is located at the geometric center of the rotor hub (coincident at point O). The rotor rotates at speed Ω.

Both body and rotor head are joined by a rigid shaft, and aerodynamic forces on the blades are not taken into account. Such assumption is quite realistic since the helicopter is on the ground and it adequately predicts the instabilities for an articulated rotor system [11]. In this work, the rotor is composed of $N_b = 4$ blades.

By applying Lagrange's equation on the expression of energies and work of the dynamical system, the equations of motion with respect to $\mathbf{u}$, which represents the degrees of freedom of the mechanical model, are given by

$$\mathbf{M}\ddot{\mathbf{u}} + \mathbf{G}\dot{\mathbf{u}} + \mathbf{K}\mathbf{u} = \mathbf{F}_{\mathbf{ext}} \tag{1}$$

where

$$\mathbf{M}(t) = \begin{pmatrix} 1 & 0 & -r_{m1}\sin(\psi_1) & -r_{m2}\sin(\psi_2) & -r_{m3}\sin(\psi_3) & -r_{m4}\sin(\psi_4) \\ 0 & 1 & r_{m1}\cos(\psi_1) & r_{m2}\cos(\psi_2) & r_{m3}\cos(\psi_3) & r_{m4}\cos(\psi_4) \\ -r_{b1}\sin(\psi_1) & r_{b1}\cos(\psi_1) & 1 & 0 & 0 & 0 \\ -r_{b2}\sin(\psi_2) & r_{b2}\cos(\psi_2) & 0 & 1 & 0 & 0 \\ -r_{b3}\sin(\psi_3) & r_{b3}\cos(\psi_3) & 0 & 0 & 1 & 0 \\ -r_{b4}\sin(\psi_4) & r_{b4}\cos(\psi_4) & 0 & 0 & 0 & 1 \end{pmatrix} \tag{2}$$

$$\mathbf{G}(t) = \begin{bmatrix} r_{c1} & 0 & -2\Omega r_{m1}\cos(\psi_1) & -2\Omega r_{m2}\cos(\psi_2) & -2\Omega r_{m3}\cos(\psi_3) & -2\Omega r_{m4}\cos(\psi_4) \\ 0 & r_{c2} & -2\Omega r_{m1}\sin(\psi_1) & -2\Omega r_{m2}\sin(\psi_2) & -2\Omega r_{m3}\sin(\psi_3) & -2\Omega r_{m4}\sin(\psi_4) \\ 0 & 0 & r_{c3} & 0 & 0 & 0 \\ 0 & 0 & 0 & r_{c4} & 0 & 0 \\ 0 & 0 & 0 & 0 & r_{c5} & 0 \\ 0 & 0 & 0 & 0 & 0 & r_{c6} \end{bmatrix} \tag{3}$$

$$\mathbf{K}(t) = \begin{pmatrix} \omega_x^2 & 0 & \Omega^2 r_{m1}\sin(\psi_1) & \Omega^2 r_{m2}\sin(\psi_2) & \Omega^2 r_{m3}\sin(\psi_3) & \Omega^2 r_{m4}\sin(\psi_4) \\ 0 & \omega_y^2 & -\Omega^2 r_{m1}\cos(\psi_1) & -\Omega^2 r_{m2}\cos(\psi_2) & -\Omega^2 r_{m3}\cos(\psi_3) & -\Omega^2 r_{m4}\cos(\psi_4) \\ 0 & 0 & \omega_{b1}^2 + \Omega^2 r_{a1}^2 & 0 & 0 & 0 \\ 0 & 0 & 0 & \omega_{b2}^2 + \Omega^2 r_{a2}^2 & 0 & 0 \\ 0 & 0 & 0 & 0 & \omega_{b3}^2 + \Omega^2 r_{a3}^2 & 0 \\ 0 & 0 & 0 & 0 & 0 & \omega_{b4}^2 + \Omega^2 r_{a4}^2 \end{pmatrix} \tag{4}$$

$$\mathbf{F}_{\text{ext}}(t) = \begin{pmatrix} \sum_{k=1}^{N_b} \Omega^2 r_{mk}\left(\frac{a+b}{a}\right)\cos(\psi_k) \\ \sum_{k=1}^{N_b} \Omega^2 r_{mk}\left(\frac{a+b}{a}\right)\sin(\psi_k) \\ 0 \\ 0 \\ 0 \\ 0 \end{pmatrix} \tag{5}$$

M, **G**, and **K** correspond to the mass, damping and stiffness matrix, respectively. They are nonsymmetric and nondiagonal matrices due to the presence of periodic terms. $\mathbf{F}_{\mathbf{ext}}$ is equal to zero if all blades have the same inertial and geometrical properties.

The matrices then expressed in Eq. (1) are written in the same form as presented in Refs. [9,10], except for diagonal elements of the damping matrix **G**. These terms are related to the presence of viscous dampers in the helicopter, where

$$r_{c1..2} = \frac{C_{X..Y}}{m_f + \sum_{k=1}^{N_b} m_{bk}}, \quad r_{ck+2} = \frac{C_{bk}}{b^2 m_{bk} + I_{z_{bk}}}, \quad k = 1..4$$

The factors $r_{c1..2}$ are ratios between the damping coefficient of the fuselage in x and y directions, respectively, and the total helicopter mass, whereas $r_{c3..6}$ are ratios between the damping coefficient and the total inertia of blade rotational motion.

The terms ω_x and ω_y represent the resonance frequencies of the fuselage in directions x and y, respectively. Moreover, $\omega_{b3..6}$ are the lead-lag resonance frequencies of blades from 1 to 4.

2.2 Stability Analysis. Floquet's theory is used to predict the boundaries of instability of the ground resonance phenomenon [2,4,9,10,12,13], represented by the periodic equations in Eq. (1).

According to Ref. [14] and based on the Floquet's theory [15], there is a transition matrix Φ that links the state vector $\mathbf{v}$ at two different moments, t_0 and t, i.e., from $\mathbf{v}(t_0)$ to $\mathbf{v}(t)$.

The stability of the dynamical system is given by the monodromy matrix $\mathbf{R}$ or the floquet transition matrix (FTM) defined as

$$\mathbf{R} = \Phi(t_0 + T, t_0) \tag{6}$$

where T is the period of the equations in Eq. (1).

A special technique, called Picard interactions, is devoted to the numerical computation of the monodromy matrix [16]. The periodic state-space system $S(t)$ can be approximated by a series of p step functions during a period. Thus,

$$1\mathbf{R} = \prod_{k=1}^{p} e^{\mathbf{S}_k (t_k - t_{k-1})} \tag{7}$$

where matrix $\mathbf{S}_k$, within the interval defined by t_k and t_{k-1}, is a constant value of $\mathbf{S}(t)$ at $t = t_{k-1}$.

The stability of Eq. (1) is given by the eigenvalues λ of the monodromy matrix $\mathbf{R}$. If the norm of the eigenvalues, named characteristic multiplier, is less than one, the mechanical system is stable.

Accordingly to Ref. [14], the maximum amplitude of the multiplier characteristic $|\lambda|$ at each critical region is related to the system exponential growth rate. High value for system exponential growth rate claims for higher damping level.

3 Experimental Setup

An experimental setup was designed and developed to reproduce the unstable motion of helicopters under the ground resonance phenomenon, contributing towards the physical understanding of the phenomenon and validating the theoretical results.

3.1 Description. The conceptual design of the experimental aircraft is based on the same mechanisms and hypotheses considered for the mechanical system, described in Sec. 2.1 and in Refs. [9,10]. Figure 2 is an illustration of the final design of the experimental helicopter.

The rotor head is composed of four rigid blades assembled with a rigid rotor hub. Each blade has, independently, lead-lag oscillations along a vertical axis, passing through point B. Flexible laminas under bending oscillations, in which it is attached (i.e., clamped) at each of its extremities to the rotor hub and to the blade, gives the blade angular spring stiffness. The driven torque needed to rotate the rotor system at a constant angular speed Ω is obtained using an electric motor.

The electric motor is linked to a chassis and both elements (motor and chassis) make up the fuselage system. Four laminas, called fuselage laminas, are linked to the chassis. The fuselage

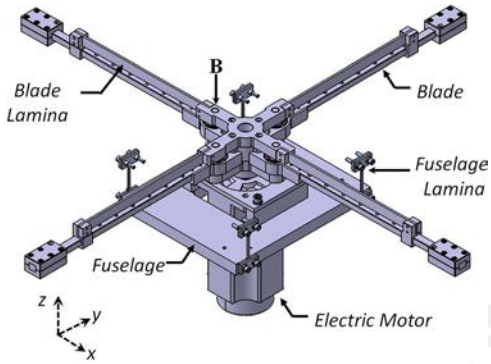

Fig. 2 The final design of the experimental helicopter for ground resonance analysis

(a)

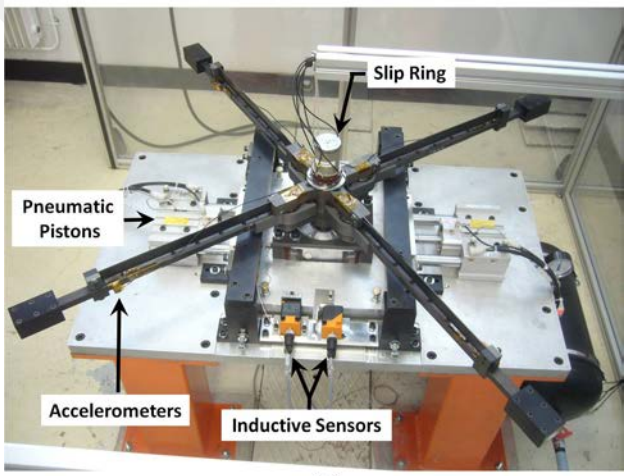

(b)

Fig. 3 The experimental setup: (*a*) global view and (*b*) detailed view

laminas, when later linked to inertial rigid beams (see Fig. 3(*b*)), will support the whole weight of the experimental helicopter.

The fuselage, suspended over an inertial table, can oscillate in both longitudinal and lateral directions (i.e., x and y directions, respectively). Similar to the blades, the spring stiffness of the helicopter landing skids is given by the fuselage laminas. The kinematic couplings at each lamina joint are of clamped-clamped type.

The spring stiffness of the fuselage and blades is strongly dependent on the lamina geometry, when they are made of the same

Table 1 Data of the experimental helicopter (EH)

System	Description	Units	Value
Fuselage	m_f	kg	45.2
Rotor	$m_{b\ 1.4}$	kg	2.84
	a	m	0.1
	b	m	0.22
	I_{zb}	kg m^2	0.11
Machine	Length	m	1.28
	Width	m	1.28
	Height	m	1.00

material. Three sets of laminas intended to study different helicopter configurations (by altering the spring stiffness) are used for the blades.

The numerical data of the experimental helicopter (EH) are shown in Table 1, as well as the main dimensions of the whole machine, including the inertial table. The transparent safety enclosure cabinet, the pneumatic pistons and the inductive sensors are elements of the security system (see Fig. 2). The maximum allowable rotor speed and the maximum longitudinal displacement of the fuselage are 600 rpm and 2 mm, respectively.

3.2 Measurement System. The measurement system aims to record the fuselage and blade oscillations in order to identify the critical rotor speeds which determine the boundaries of the unstable zone by analyzing the temporal responses.

Accelerometers are used to measure the longitudinal acceleration of the fuselage and the angular acceleration of each blade. The revolving rotor speed is obtained using an optical encoder located in the motor. The slip ring element allows the signal to be transferred from a rotating to a fixed frame (see Fig. 3(*b*)). A data acquisition system records the measured signals during an experimental test. The boundary of an instability zone is determined experimentally by identifying two aspects: high amplitude of vibration after a certain time, and the envelope of the measured signals growths exponentially.

A low-pass butterworth filter is applied (cutoff frequency = 20 Hz and order = 5) to the measured signals in order to minimize the influence (i.e., high frequencies) of the magnetic field provided by the electric motor on the accelerometers.

3.3 Spring Stiffness Determination. By considering the fuselage and blade as uncoupled oscillators, their equivalent spring stiffness is determined dynamically using their natural frequencies of vibration. The natural frequencies are obtained from their free oscillations ($\Omega = 0$), when they are shifted from their equilibrium point independently.

Figure 4 shows the temporal response of a blade fitted with set 1 of blade laminas and its spectrum diagram.

In this case, the frequency spectrum diagram shows three peaks at 2.25, 4.83, and 7.08 Hz on the power spectrum, identifying the nonlinear behavior of the blades (nonlinear spring stiffness). The linear equivalent blade spring stiffness is determined by considering the natural blade frequency equal to that with the maximum power spectrum peak (i.e., at 2.25 Hz).

Both blade and fuselage natural frequencies are then obtained by repeating this same process. The values obtained are shown in subsequent sections.

Moreover, the structural damping factor is determined by analyzing the exponential rate decay of the oscillations. A mean structural damping factor of 0.2% is found for the blades and fuselage.

4 Numerical Versus Experimental Results

Two different approaches, numerical and experimental, were used for the study of the ground resonance phenomenon for isotropic (IR) and anisotropic (AR) rotors. In the IR configurations, all blades are fitted with the same set of blade laminas, while in the AR configuration, one blade is fitted with a lamina from a different set with respect to the others.

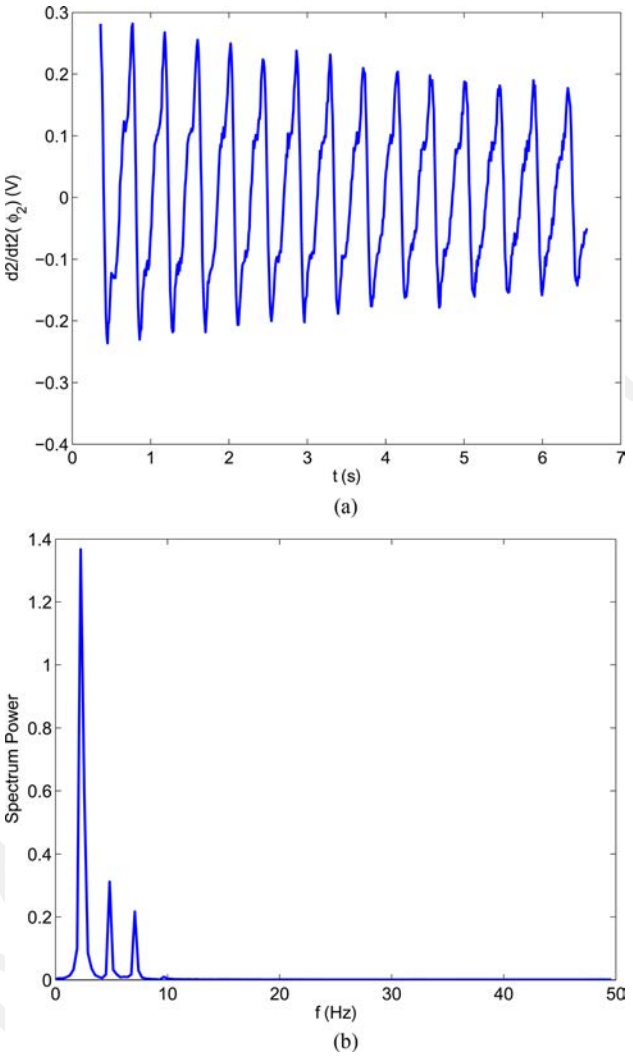

Fig. 4 Blade oscillations with set 1 of blade laminas in panel (*a*) and its frequency spectrum diagram in panel (*b*)

Table 2 IR and AR rotor configurations: natural blade frequency and the set of laminas of each blade

Blade k		1	2	3	4
IR	Set of lamina	2	2	2	2
	ω_{bk} (Hz)	3.19	3.14	3.47	3.07
AR	Set of lamina	1	1	1	2
	ω_{bk} (Hz)	2.49	2.39	2.35	3.25

Table 2 indicates the set of blade laminas used for each rotor configuration studied, as well as the blade natural frequency determined by following the procedure described in Sec. 3.3.

Even considering the same set of blade laminas (IR configuration), differences on blade-to-blade natural frequencies are verified. This fact might be explained by slight variations of the young's modulus of the material of the blade laminas or by the boundaries conditions imposed by the fixation of the laminas on the blades which may vary from each blade.

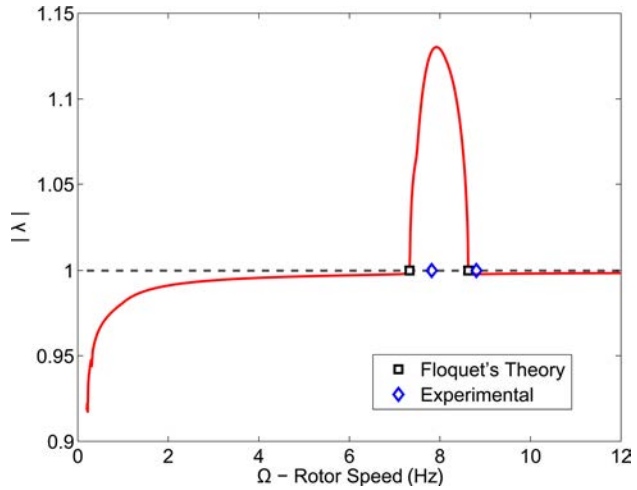

Fig. 5 Comparison between the numerical and experimental instability prediction for IR configuration

Table 3 Boundaries of instability found using FM and those determined experimentally for IR configuration

	With FM	Experimental	Deviation (%)
Lower bound	7.33	7.82	6.68
Upper bound	8.63	8.80	1.97

Concerning the equivalent spring stiffness of the fuselage, the natural frequencies identified are $\omega_x = 2.55$ Hz and $\omega_y = 15.8$ Hz in the longitudinal and lateral directions, respectively.

It is important to note that the numerical analyses using Floquet's theory are conducted by assuming the period divisions $p = 64$ parts.

4.1 Isotropic Rotor (IR). Considering the data described in the previous sections about the experimental helicopter with IR rotor configuration, Fig. 5 shows the evolution of the characteristic multiplier (curved line) with respect to the angular rate Ω. The predicted boundaries of instability are represented by the square symbols, whereas that determined experimentally (see Sec. 3.2) is shown using diamonds. Table 3 presents their numerical values.

The instability region, at which the ground resonance phenomenon occurs for isotropic rotor, is related to the coalescence between two modes of vibration of the helicopter (i.e., the fuselage mode and a rotor mode) [2].

The existence of only one instability zone (i.e., zone where the characteristic multiplier is greater than the unit) is observed, even if the helicopter has two distinct fuselage natural frequencies. This is explained by the limitation of the experimental setup (maximum allowable rotor speed is 600 rpm).

The boundaries of instability verified experimentally are correlated with respect to those predicted numerically. A maximum deviation of 6.68% is presented. This difference might be reduced by optimizing the experimental procedure to determine the boundaries of instability: find the instant when the exponential growth rate of the measured signal becomes positive.

Regarding the fuselage and blade accelerations measured of the experimental helicopter in a critical zone, it is possible to verify the exponential growth of the envelope of those signals (see Fig. 6). Evidence of the presence of an instability is thus provided.

Accordingly to Ref. [14], the system exponential growth rate at the critical region ($\Omega_{cr} = 7.5$ Hz) is related to $\max(|\lambda|) = |\lambda_{cr}| \approx 1.12$.

A general representation of the rotor deformation shape 1s before the fuselage reaches the maximum longitudinal displacement is given in Fig. 7. The black lines represent the blade, whereas the gray dashed line is the origin of the blade lead-lag angle. In all cases, a shift of the rotor center of mass from the vertical rotating axis is verified.

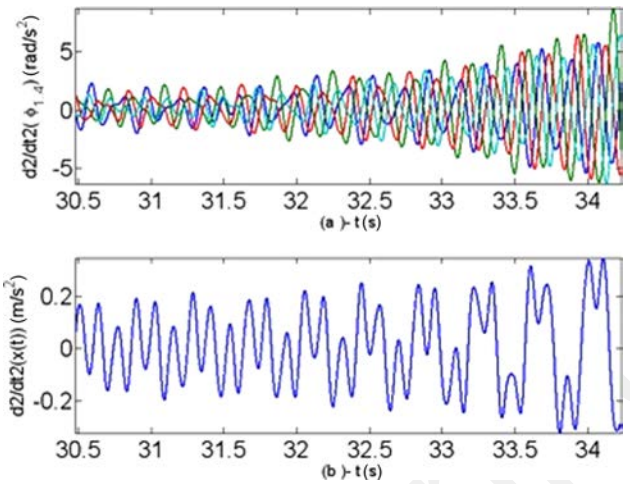

Fig. 6 Time history of the experimental helicopter with IR configuration at $\Omega \approx 7.5$ Hz; (*a*) blades and (*b*) fuselage accelerations

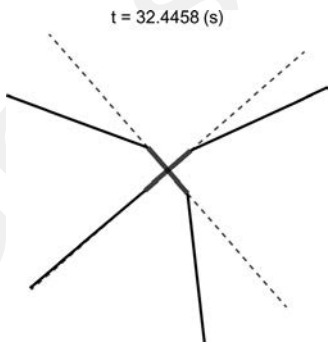

Fig. 7 Rotor deformation shape for the experimental helicopter EH with IR at $\Omega \approx 7.5$ Hz

It is important to note that the lead-lag angles on the figure are only illustrative, since they are slightly increased for didactic reasons.

4.2 Anisotropic Rotor (AR). The study of anisotropic rotors is very interesting from a practical point of view. Indeed, the effects of aging or failure of mechanical elements may alter the spring stiffness of blades and consequently change the boundaries of instability of the ground resonance phenomenon.

Parametric studies have been done recently and they illustrate the evolution of the boundaries of instabilities as a function of the blade stiffness asymmetries affected in different blades [9,10].

The present work concerns the study of an arbitrary case of asymmetric rotors. The blade lead-lag natural frequency of one blade is slightly increased (see AR in Table 2), having the lag stiffness similar to those blades of the isotropic rotor.

It is important to remark that this case is similar to that in which three blades are asymmetric (i.e., lag stiffness level decreased) with respect to the reference blade (i.e., blade n°4).

The evolution of the characteristic multiplier (curved line) with respect to the angular rate Ω, obtained by using Floquet's theory, is shown in Fig. 8. The predicted boundary of instability is represented by the square symbols, whereas that determined experimentally is shown using diamonds. Table 4 presents their numerical values.

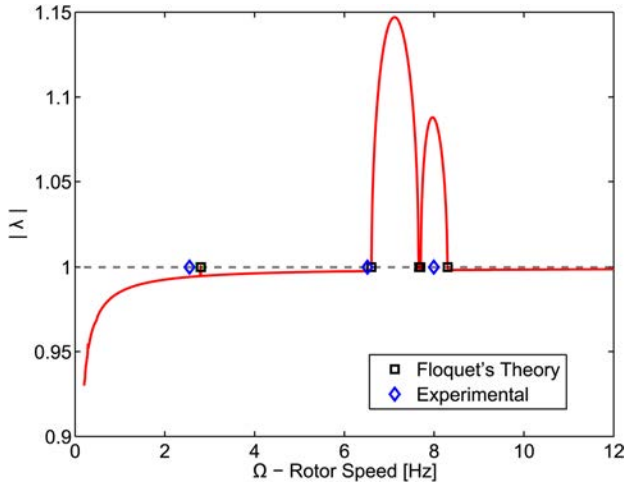

Fig. 8 Comparison between the numerical and experimental instability prediction for AR configuration

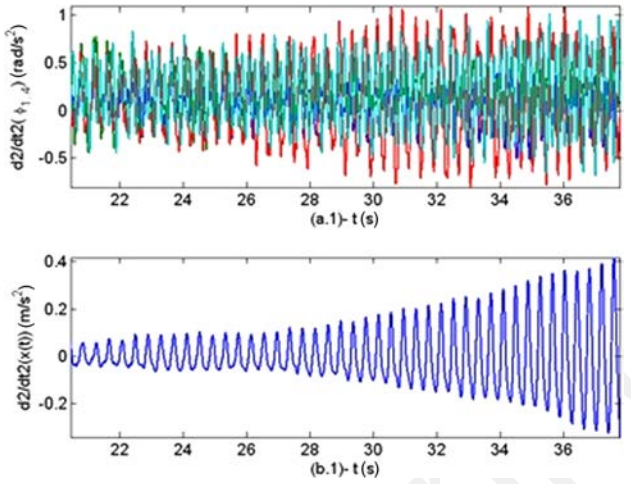

Fig. 9 Time history of the experimental helicopter with AR configuration at $\Omega \approx 2.5$ Hz; (*a*) blades and (*b*) fuselage accelerations

Table 4 Boundaries of instability found using FM and those determined experimentally for AR configuration

Zone		With FM	Experimental	Deviation (%)
1	—	2.81	2.55	9.20
2	Lower bound	6.60	6.51	1.36
	Upper bound	7.66	—	—
3	Lower bound	7.69	—	—
	Upper bound	8.30	7.99	3.73

Three instability zones are predicted with Floquet's theory in the case of one dissimilar blade. It is important to note that the analysis is conducted until the maximum allowable rotor speed of the experimental helicopter is reached.

Two new instability zones (i.e., zones 1 and 2) are observed when compared to an isotropic rotor. The third zone corresponds to the same critical zone found with the IR configuration.

Experimentally, only zone 1 and the lower and upper limits of zones 2 and 3, respectively, were able to be determined due to the resolution of the electric motor. The stable zone between zone 2 and 3 was not found due to their proximity.

Regarding the maximum amplitude of $|\lambda|$ at each critical region, the zone 1 seems to be very sensible to dissipative efforts once the exponential growth rate is very low [14].

By introducing blade stiffness asymmetries in three blades, a decrement of the exponential growth rate is observed (with respect to IR configuration). The $\max(|\lambda|) \approx 1.12$ for IR while $\max(|\lambda|) \approx 1.08$ for AR (zone 3). However, the new critical zone 2 has an exponential growth rate (i.e., $\max(|\lambda|) \approx 1.145$) bigger than that observed with isotropic rotor.

Analytical asymptotic has been developed on the helicopter equations of motion. The periodic terms (i.e., the coupling terms) were considered as parametric excitation of the uncoupled fuselage-rotor dynamic system [10].

The analysis carried out on the parametrically excited dynamic system leads to the existence of parametric resonances of first and second order, in which some of them are unstable.

At parametric instabilities of first order, the fuselage is in resonance with the blade(s) and vice versa. It evidences thus the coalescence of the fuselage and rotor modes of vibration at the instabilities. The critical rotor speed, at which the parametric instabilities take place, is given by linear function (i.e., sum and difference) between the natural frequencies of the fuselage and blade.

These instabilities are found in isotropic and anisotropic (zones 2 and 3) rotors. In isotropic rotor configuration all blades are in resonance with the fuselage, since the lag natural frequency of the blades are similar. Regarding AR, at zone 2 three blades are in resonance with the fuselage, and at zone 3 only one blade is in resonance.

Regarding the parametric instabilities of second order, analytical developments evidence that fuselage is in resonance with their own vibration. The critical rotor speeds are given as a function of the fuselage natural frequencies. These instabilities happens only in AR.

The zone 1 in AR evidence parametric instabilities of second order and it happens at $\Omega_{cr} = 2.81$ Hz which is close to $\omega_x = 2.25$ Hz. Figure 9 illustrates, at initial time intervals, the exponential growth of the envelope of only the fuselage acceleration. It evidences the fact of only the fuselage is in resonance at the unstable region.

5 Conclusions

The dynamics of helicopters on the ground, but under the aging or damage effects, have recently been studied. In fact, these effects may result in the spring stiffness of blades varying randomly, compromising the nominal operation of the aircraft and leading the aircraft to the ground resonance phenomenon. The investigations predict the existence of new instability zones with high asymmetries between blades.

A new experimental setup, designed to experimentally reproduce the ground resonance phenomenon for isotropic and anisotropic rotors, to further comprehend this phenomenon and to validate the theoretical results (verifying the existence of new instabilities regions for anisotropic rotors with respect to the isotropic ones), has been described and presented.

The conceptual design of the apparatus was based on the same mechanisms and hypotheses considered for the simplified helicopter with hinged blades, used for the theoretical analysis. Efforts were made to obtain an easily adjustable parametric system (i.e., blade mass, blade, and fuselage spring stiffness). During an experimental test, the acceleration signals of the fuselage and the blade lead-lag rotations were recorded.

For both approaches, numerical (i.e., Floquet's Theory) and experimental, the boundaries of instability found were quite similar for isotropic and anisotropic rotor configurations.

The appearance of new instability zones in anisotropic rotors with respect to isotropic ones was verified experimentally, as predicted theoretically. This fact was evidenced by the exponential divergence of the measured signals, which characterizes the unstable oscillations during the occurrence of the phenomenon.

Nomenclature

a = rotor eccentricity
b = blade equivalent length

$\mathbf{F_{ext}}$ = external force vector
$\mathbf{G}$ = damping matrix of the dynamical system
I_{Zbk} = lag rotational inertia of the kth blade around its center of gravity
$\mathbf{K}$ = stiffness matrix of the dynamical system
K_{bk} = kth blade lead-lag stiffness
K_{fx}, K_{fy} = longitudinal and transverse stiffness of fuselage
m_f, m_{bk} = fuselage and mass of kth blade
$\mathbf{M}$ = mass matrix of the dynamical system
N_b = number of blades in the rotor
$r_{ak} = \sqrt{ar_{bk}}$
r_{bk} = ratio between the static moment over the total lead-lag rotational inertia of the kth blade
r_{mk} = ratio between the static moment of the kth blade over the total mass of the helicopter
$\mathbf{S}$ = state space matrix
t = time
$\mathbf{u}$ = vector of degree of freedom of the system
$\mathbf{v}$ = state vector
$x(t)$, $y(t)$ = longitudinal and transverse displacement of the fuselage
(x, y, z) = mobile coordinate system attached to the rotor hub
(X_0, Y_0, Z_0) = inertial referential coordinate system
$\varphi_k(t)$ = lead-lag angle of kth blade
Φ = transition matrix (Floquet's Theory)
Ω = rotor speed
ζ_k = azimuth angle for the kth blade
ω_{bk} = lead-lag natural frequencies of kth blade at rest
ω_x, ω_y = fuselage natural frequencies in x and y directions

Appendix: Energy Expressions

The kinetic and potential energy expressions and the work expression of dissipative forces of the dynamical system are presented as follows separately. They are all written on the inertial reference frame.

Kinetic Energy. The kinetic energy of the whole dynamical system consists in the sum of kinetic energy expression of fuselage T_{Fus} and rotor head T_{RH} systems. These energies are given below:

$$T_{\text{Fus}} = \frac{m_f}{2}\left(\dot{x}^2(t) + \dot{y}^2(t)\right) \tag{A1}$$

$$T_{\text{RH}} = \frac{1}{2}\sum_{k=1}^{N_p}\left[I_{z_{bk}}\dot{\varphi}_k^2 + m_{bk}\left(\dot{x}_{bk}^2 + \dot{y}_{bk}^2\right)\right] \tag{A2}$$

$$= \frac{1}{2}\sum_{k=1}^{N_p} I_{z_{bk}}\dot{\varphi}_k^2 + \frac{1}{2}m_{bk}\sum_{k=1}^{N_p}\left\{\begin{array}{c}(\dot{x}+\dot{y}) + b^2\dot{\varphi}_k^2 + 2b^2\Omega\dot{\varphi}_k + b^2\Omega^2(a^2+b^2) \\ 2ab\cos(\varphi_k)\left[\Omega^2 + \Omega\dot{\varphi}_k\right] + 2a\Omega[-\dot{x}\sin(\psi_k) + \dot{y}\cos(\psi_k)] \\ 2b(\Omega\dot{y} + \dot{y}\dot{\varphi}_k)\cos(\psi_k+\varphi_k) - 2b(\Omega\dot{x} + \dot{x}\dot{\varphi}_k)\sin(\psi_k+\varphi_k)\end{array}\right\} \tag{A3}$$

Potential Energy. The potential energy of the whole dynamical system consists in the sum of potential energy of fuselage U_{Fus} and rotor head U_{RH} systems. The expressions of these energies are given below:

$$U_{\text{Fus}} = \frac{1}{2}\left(K_{fX}x^2 + K_{fY}y^2\right) \tag{A4}$$

$$U_{\text{RH}} = \frac{1}{2}\sum_{k=1}^{N_p} K_{bk}\varphi_k^2 \tag{A5}$$

Work of Dissipative Forces. The work of dissipative forces of the whole dynamical system consists in the sum of the work done by dissipative forces acting on the fuselage δF_{Fus} and rotor head δF_{RH} systems. They are given below as:

$$U_{\text{Fus}} = \frac{1}{2}\left(C_{fX}\dot{x}^2 + C_{fY}\dot{y}^2\right) \tag{A6}$$

$$U_{RH} = \frac{1}{2}\sum_{k=1}^{N_p} C_{bk}\dot{\varphi}_k^2 \tag{A7}$$

References

[1] Coleman, R. P., and Feingold, A. M., 1957, "Theory of Self-Excited Mechanical Oscillations of Helicopter Rotors With Hinged Blades," NASA Technical Report TN 3844.

[2] Wang, J., and Chopra, I., 1992, "Dynamics of Helicopters in Ground Resonance With and Without Blade Dissimilarities," AIAA Dynamics Specialists Conference, Dallas, TX, April 16–17, AIAA Paper No. 92-1208, pp. 273–291.

[3] Donham, R., Cardinale, S., and Sachs, I., 1969, "Ground and Air Resonance Characteristics of a Soft In-Plane Rigid-Rotor System," J. Am. Helicopter Soc., **14**, p. 33–41.

[4] Hammond, C., 1974, "An Application of Floquet Theory to Prediction of Mechanical Instability," J. Am. Helicopter Soc., **19**, p. 14–23.

[5] Hodges, D., 1979, "An Aeromechanical Stability Analysis for Bearingless Rotor Helicopters," J. Am. Helicopter Soc., **24**, p. 2–9.

[6] Gandhi, F., and Malovrh, B., 1999, "Influence of Balanced Rotor Anisotropy on Helicopter Aeromechanical Stability," AIAA J., **37**(10), pp. 1152–1160.

[7] Gandhi, F., and Chopra, I., 1994, "An Analytical Model for a Nonlinear Elastomeric Lag Damper and Its Effect on Aeromechanical Stability in Hover," J. Am. Helicopter Soc., **39**(4), pp. 59–69.

[8] Gandhi, F., Wang, K. W., and Xia, L., 2001, "Magnetorheological Fluid Damper Feedback Linearization Control for Helicopter Rotor Application," Smart Mater. Struct., **10**(1), pp. 96–103.

[9] Sanches, L., Michon, G., Berlioz, A., and Alazard, D., 2011, "Instability Zones for Isotropic and Anisotropic Multibladed Rotor Configurations," Mech. Mach. Theory, **46**(8), pp. 1054–1065.

[10] Sanches, L., Michon, G., Berlioz, A., and Alazard, D., 2012, "Parametrically Excited Helicopter Ground Resonance Dynamics With High Blade Asymmetries," J. Sound Vib., **331**(16), pp. 3897–3913.

[11] Chopra, I., 1989, "Perspectives in Aeromechanical Stability of Helicopter Rotors," AHS National Specialists' Meeting on Rotorcraft Dynamics, Arlington, TX, November 13–14.

[12] Skjoldan, P., and Hansen, M., 2009, "On the Similarity of the Coleman and Lyapunov-Floquet Transformations for Modal Analysis of Bladed Rotor Structures," J. Sound Vib., **327**(3–5), pp. 424–439.

[13] Sanches, L., Michon, G., Berlioz, A., and Alazard, D., 2009, "Modélisation Dynamique d'un Rotor sur Base Flexible," Congress Français de Mécanique, Marseille, France, August 24–28.

[14] Bauchau, O., and Nikishkov, Y., 2001, "An Implicit Floquet Analysis for Rotorcraft Stability Evaluation," J. Am. Helicopter Soc., **46**(3), pp. 200–209.

[15] Floquet, G., 1883, "Sur les Équations Différentielles Linéaires à Coefficients Périodiques," Ann. Sci. Ecole Norm. Sup., **2**(12), pp. 47–88.

[16] Dufour, R., and Berlioz, A., 1998, "Parametric Instability of a Beam Due to Axial Excitations and to Boundary Conditions," ASME J. Vibr. Acoust., **120**(2), pp. 461–467.